Getting drugs through small pores: Exploiting the porins pathway in *Pseudomonas aeruginosa.*

Authors: Susruta Samanta[1,5], Igor Bodrenko[1], Silvia Acosta-Gutiérrez[1], Tommaso D'Agostino[1], Monisha Pathania[2], Ishan Ghai[3], Christian Schleberger[4], Dirk Bumann[4], Richard Wagner[3], Mathias Winterhalter[3], Bert van den Berg[2], Matteo Ceccarelli[1*]

Affiliations:

[1]Department of Physics, University of Cagliari, SP Monserrato-Sestu Km 0.8, Monserrato, 09042, Italy.

[2]Institute for Cell and Molecular Biosciences, The Medical School, Newcastle University, Newcastle upon Tyne, NE2 4HH, United Kingdom.

[3]Department of Life Sciences and Chemistry, Jacobs University Bremen, 28719 Bremen, Germany.

[4]Biozentrum, University of Basel, Klingelbergstrasse 50/70, CH-4056 Basel, Switzerland

[5]Department of Chemistry, Manipal University Jaipur, VPO Dehmi Kalan, Jaipur, PIN–303007, Rajasthan, India.

Corresponding author's email address: matteo.ceccarelli@dsf.unica.it

Supplementary Information

Pages: 23

Figures: 10

Tables: 1

Figure S1a: Sequence alignment of OccK8 with all other known members of the OccK family. No other member of the family has a positive residue in the position corresponding to K327 (shown in blue rectangle). K327 forms salt bridge with D311 (shown with a red arrow), which is also absent in all other OccK family members. This indicates that this salt bridge (Gate A) is unique in OccK8. The residue D322 is shown with a blue arrow.

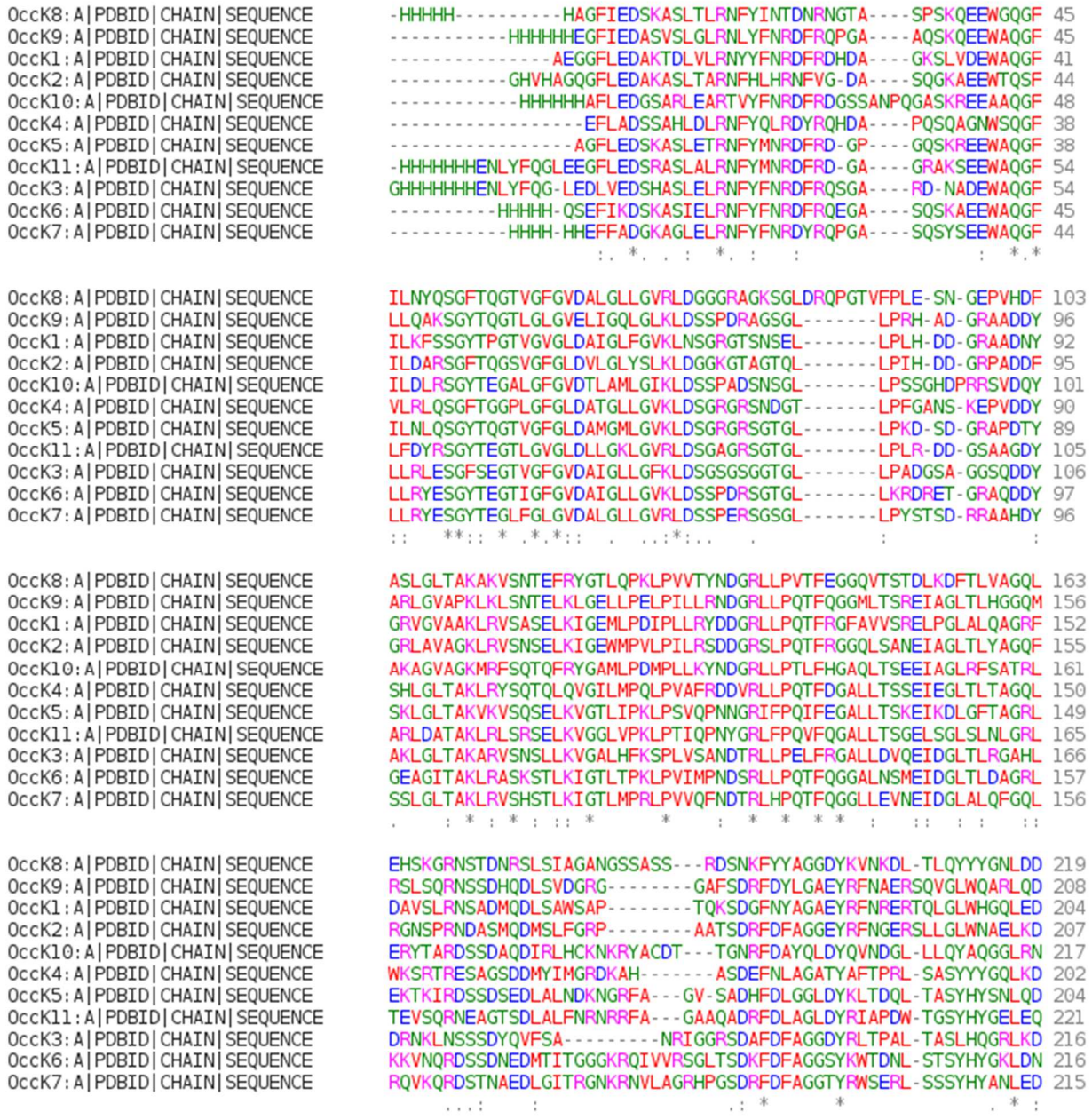

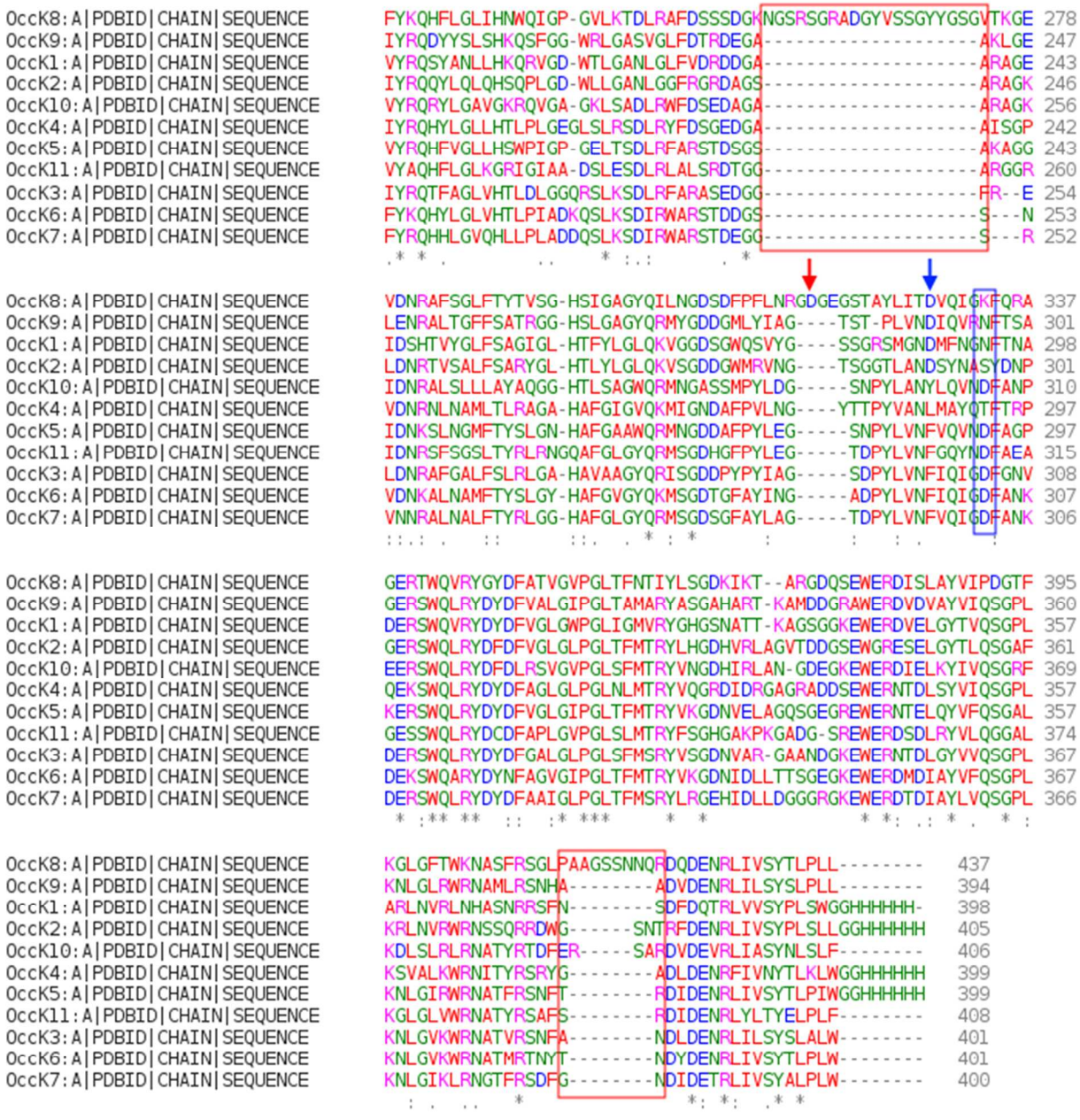
OccK8:A|PDBID|CHAIN|SEQUENCE FYKQHFLGLIHNWQIGP-GVLKTDLRAFDSSSDGKNGSRSGRADGYVSSGYYGSGVTKGE 278
OccK9:A|PDBID|CHAIN|SEQUENCE IYRQDYYSLSHKQSFGG-WRLGASVGLFDTRDEGA----------AKLGE 247
OccK1:A|PDBID|CHAIN|SEQUENCE VYRQSYANLLHKQRVGD-WTLGANLGLFVDRDDGA----------ARAGE 243
OccK2:A|PDBID|CHAIN|SEQUENCE IYRQQYLQLQHSQPLGD-WLLGANLGGFRGRDAGS----------ARAGK 246
OccK10:A|PDBID|CHAIN|SEQUENCE VYRQRYLGAVGKRQVGA-GKLSADLRWFDSEDAGA----------ARAGK 256
OccK4:A|PDBID|CHAIN|SEQUENCE IYRQHYLGLLHTLPLGEGLSLRSDLRYFDSGEDGA----------AISGP 242
OccK5:A|PDBID|CHAIN|SEQUENCE VYRQHFVGLLHSWPIGP-GELTSDLRFARSTDSGS----------AKAGG 243
OccK11:A|PDBID|CHAIN|SEQUENCE VYAQHFLGLKGRIGIAA-DSLESDLRLALSRDTGG----------ARGGR 260
OccK3:A|PDBID|CHAIN|SEQUENCE IYRQTFAGLVHTLDLGGQRSLKSDLRFARASEDGG----------FR--E 254
OccK6:A|PDBID|CHAIN|SEQUENCE FYKQHYLGLVHTLPIADKQSLKSDIRWARSTDDGS----------S---N 253
OccK7:A|PDBID|CHAIN|SEQUENCE FYRQHHLGVQHLLPLADDQSLKSDIRWARSTDEGG----------S---R 252
OccK8:A|PDBID|CHAIN|SEQUENCE VDNRAFSGLFTYTVSG-HSIGAGYQILNGDSDFPFLNRGDGEGSTAYLITDVQIGKFQRA 337
OccK9:A|PDBID|CHAIN|SEQUENCE LENRALTGFFSATRGG-HSLGAGYQRMYGDDGMLYIAG----TST-PLVNDIQVRNFTSA 301
OccK1:A|PDBID|CHAIN|SEQUENCE IDSHTVYGLFSAGIGL-HTFYLGLQKVGGDSGWQSVYG----SSGRSMGNDMFNGNFTNA 298
OccK2:A|PDBID|CHAIN|SEQUENCE LDNRTVSALFSARYGL-HTLYLGLQKVSGDDGWMRVNG----TSGGTLANDSYNASYDNP 301
OccK10:A|PDBID|CHAIN|SEQUENCE IDNRALSLLLAYAQGG-HTLSAGWQRMNGASSMPYLDG-----SNPYLANYLQVNDFANP 310
OccK4:A|PDBID|CHAIN|SEQUENCE VDNRNLNAMLTLRAGA-HAFGIGVQKMIGNDAFPVLNG----YTTPYVANLMAYQTFTRP 297
OccK5:A|PDBID|CHAIN|SEQUENCE IDNKSLNGMFTYSLGN-HAFGAAWQRMNGDDAFPYLEG-----SNPYLVNFVQVNDFAGP 297
OccK11:A|PDBID|CHAIN|SEQUENCE IDNRSFSGSLTYRLRNGQAFGLGYQRMSGDHGFPYLEG-----TDPYLVNFGQYNDFAEA 315
OccK3:A|PDBID|CHAIN|SEQUENCE LDNRAFGALFSLRLGA-HAVAAGYQRISGDDPYPYIAG-----SDPYLVNFIQIGDFGNV 308
OccK6:A|PDBID|CHAIN|SEQUENCE VDNKALNAMFTYSLGY-HAFGVGYQKMSGDTGFAYING-----ADPYLVNFIQIGDFANK 307
OccK7:A|PDBID|CHAIN|SEQUENCE VNNRALNALFTYRLGG-HAFGLGYQRMSGDSGFAYLAG-----TDPYLVNFVQIGDFANK 306
OccK8:A|PDBID|CHAIN|SEQUENCE GERTWQVRYGYDFATVGVPGLTFNTIYLSGDKIKT--ARGDQSEWERDISLAYVIPDGTF 395
OccK9:A|PDBID|CHAIN|SEQUENCE GERSWQLRYDYDFVALGIPGLTAMARYASGAHART-KAMDDGRAWERDVDVAYVIQSGPL 360
OccK1:A|PDBID|CHAIN|SEQUENCE DERSWQVRYDYDFVGLGWPGLIGMVRYGHGSNATT-KAGSGGKEWERDVELGYTVQSGPL 357
OccK2:A|PDBID|CHAIN|SEQUENCE GERSWQLRYDFDFVGLGLPGLTFMTRYLHGDHVRLAGVTDDGSEWGRESELGYTLQSGAF 361
OccK10:A|PDBID|CHAIN|SEQUENCE EERSWQLRYDFDLRSVGVPGLSFMTRYVNGDHIRLAN-GDEGKEWERDIELKYIVQSGRF 369
OccK4:A|PDBID|CHAIN|SEQUENCE QEKSWQLRYDYDFAGLGLPGLNLMTRYVQGRDIDRGAGRADDSEWERNTDLSYVIQSGPL 357
OccK5:A|PDBID|CHAIN|SEQUENCE KERSWQLRYDYDFVGLGIPGLTFMTRYVKGDNVELAGQSGEGREWERNTELQYVFQSGAL 357
OccK11:A|PDBID|CHAIN|SEQUENCE GESSWQLRYDCDFAPLGVPGLSLMTRYFSGHGAKPKGADG-SREWERDSDLRYVLQGGAL 374
OccK3:A|PDBID|CHAIN|SEQUENCE DERSWQLRYDYDFGALGLPGLSFMSRYVSGDNVAR-GAANDGKEWERNTDLGYVVQSGPL 367
OccK6:A|PDBID|CHAIN|SEQUENCE DEKSWQARYDYNFAGVGIPGLTFMTRYVKGDNIDLLTTSGEGKEWERDMDIAYVFQSGPL 367
OccK7:A|PDBID|CHAIN|SEQUENCE DERSWQLRYDYDFAAIGLPGLTFMSRYLRGEHIDLLDGGGRGKEWERDTDIAYLVQSGPL 366
OccK8:A|PDBID|CHAIN|SEQUENCE KGLGFTWKNASFRSGLPAAGSSNNQRDQDENRLIVSYTLPLL-------- 437
OccK9:A|PDBID|CHAIN|SEQUENCE KNLGLRWRNAMLRSNHA--------ADVDENRLILSYSLPLL-------- 394
OccK1:A|PDBID|CHAIN|SEQUENCE ARLNVRLNHASNRRSFN--------SDFDQTRLVVSYPLSWGGHHHHHH- 398
OccK2:A|PDBID|CHAIN|SEQUENCE KRLNVRWRNSSQRRDWG------SNTRFDENRLIVSYPLSLLGGHHHHHH 405
OccK10:A|PDBID|CHAIN|SEQUENCE KDLSLRLRNATYRTDFER-----SARDVDEVRLIASYNLSLF-------- 406
OccK4:A|PDBID|CHAIN|SEQUENCE KSVALKWRNITYRSRYG--------ADLDENRFIVNYTLKLWGGHHHHHH 399
OccK5:A|PDBID|CHAIN|SEQUENCE KNLGIRWRNATFRSNFT--------RDIDENRLIVSYTLPIWGGHHHHHH 399
OccK11:A|PDBID|CHAIN|SEQUENCE KGLGLVWRNATYRSAFS--------RDIDENRLYLTYELPLF-------- 408
OccK3:A|PDBID|CHAIN|SEQUENCE KNLGVKWRNATVRSNFA--------NDLDENRLILSYSLALW-------- 401
OccK6:A|PDBID|CHAIN|SEQUENCE KNLGVKWRNATMRTNYT--------NDYDENRLIVSYTLPLW-------- 401
OccK7:A|PDBID|CHAIN|SEQUENCE KNLGIKLRNGTFRSDFG--------NDIDETRLIVSYALPLW-------- 400

Figure S1b Sequence alignment of OccK8 with other members of the Occ family – OprD, OccD3 from *Pa* and OccAB1 from *Ab*. OccK8 shares high sequence similarity with OccD1/OprD (45.7%), OccD3/OpdP (41.2%) from *Pa*, and OccAB1 (42.9%) from *Ab*. Interestingly, these porins have a negatively charged aspartate instead of a lysine at position 327.The case of K327 is highlighted with a blue box. All the other porins have acidic glutamic acid in the position corresponding to K327. The positions corresponding to D311 and D322 in OccK8 are shown with a red, and blue arrow respectively.

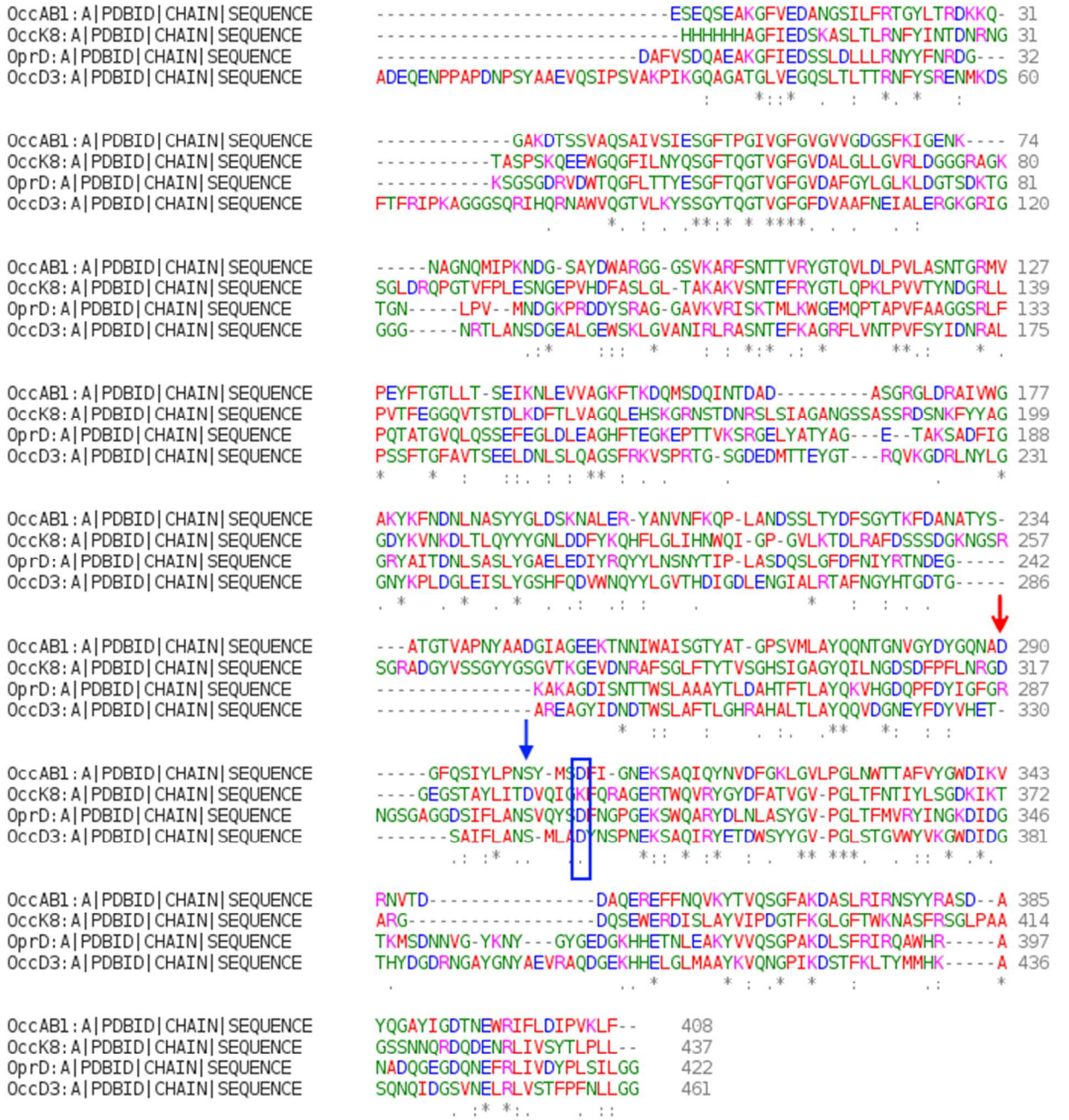

Figure S2. (Left) Distribution of minimum accessible area of OccK8 and the distribution of minimum projection area of ceftazidime. **(Right)** Comparison of available area inside OccK8 at different salt concentrations. Gate A (salt bridge interaction between D311 and K327) seems to be unstable and breaks in the presence of ions.

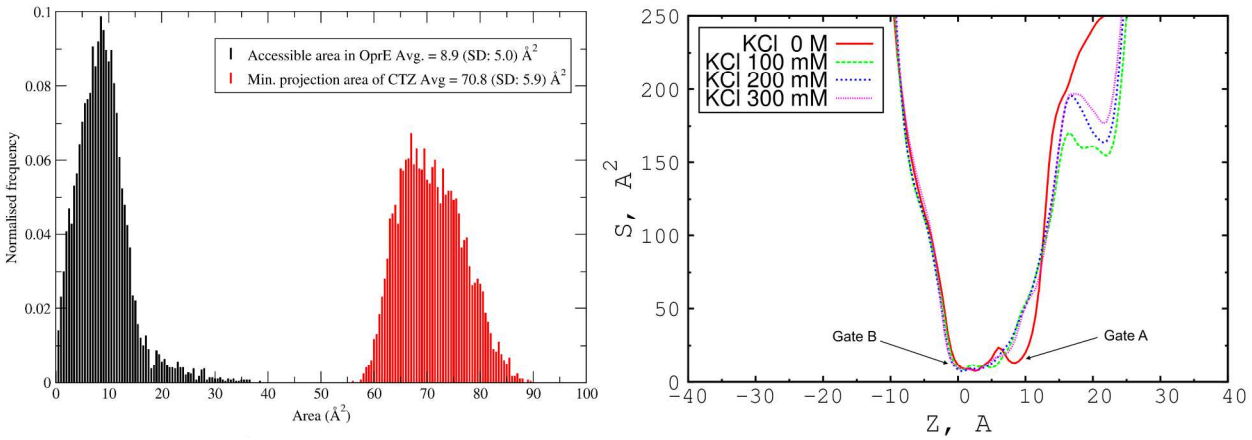

Figure S3. (left) The reconstructed free energy surface (FES) for the translocation of ceftazidime through OccK8. Both potential paths are highlighted and coloured according to the charged group of ceftazidime that faces the CR. The location of the gates is shaded and the affinity site locate near gate is indicated with a magenta star. (right) The structures corresponding to the minima (at z = 2 Å, Gate B). It consists of two states as shown in two panels. The figures on the left are the views from the side of the porin; the figures on the right are the views from the top/periplasmic side.

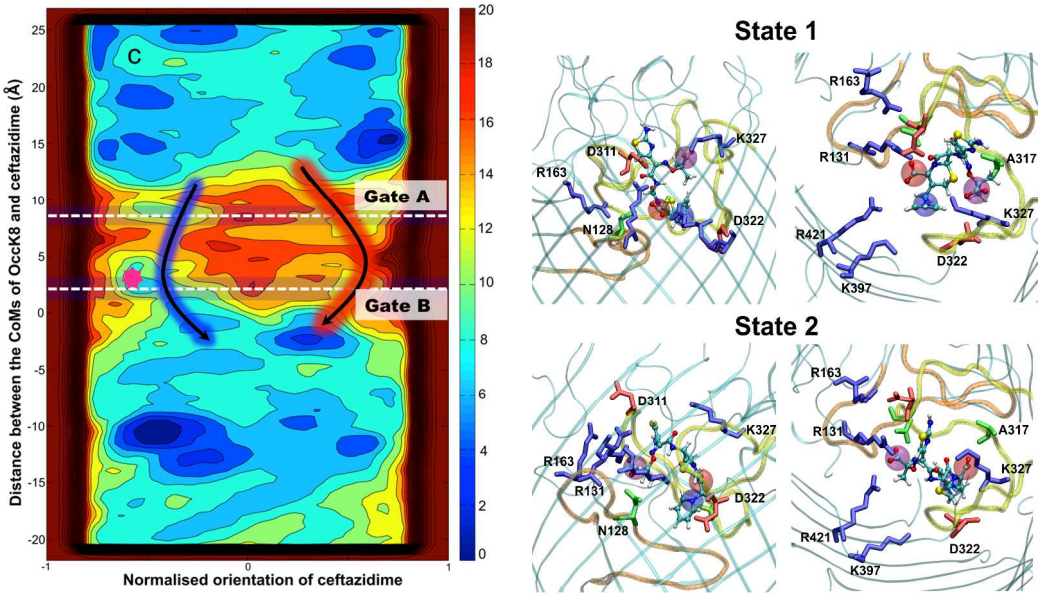

Figure S4 Molecular structure of the antibiotics investigated (top). Each molecule (bottom) is represented in licorice with its total dipole moment as a red arrow. We reported the value of the total dipole moment (in Debye) and the average size (minimal projection area in Angstrom^2), see also the open database for details: **http://www.dsf.unica.it/~gmalloci/abdb.**

Ceftazidime (25D, 68 Å^2)

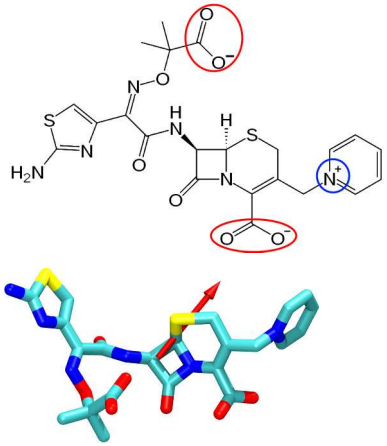

Cefepime (17.21D, 58 Å^2)

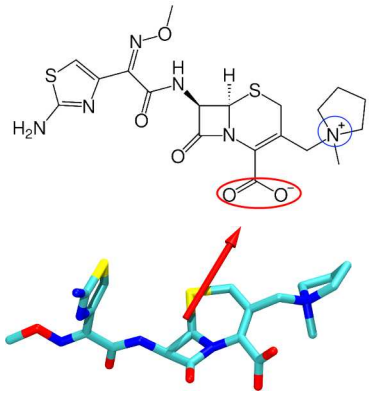

Cefotaxime (19.81D, 59 Å^2)

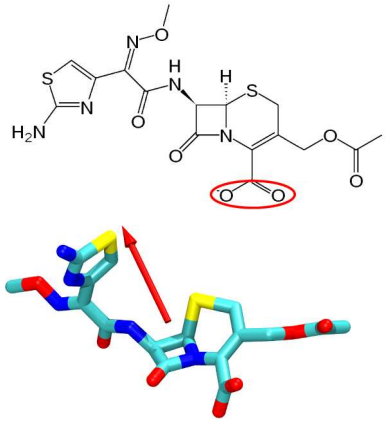

Ampicillin (35.11D, 50 Å^2)

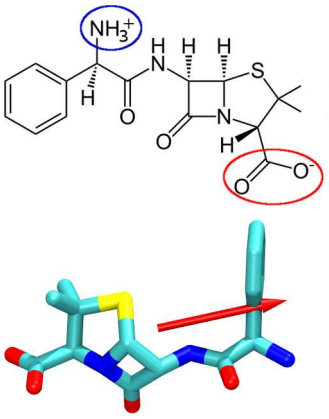

Carbenicillin (11.68D, 50 Å^2)

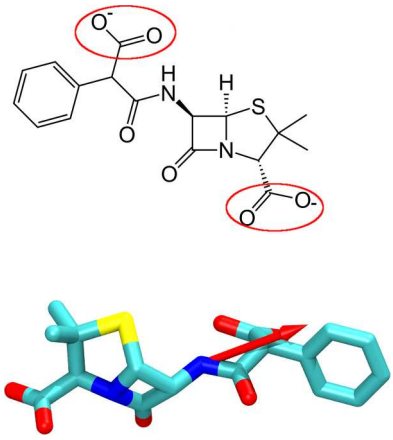

Figure S5. Distance between the positive and negative charges in the substrates during 300 ns simulation for the substrates (in the left), and 500 ns simulation for the antibiotic molecules (in the right).

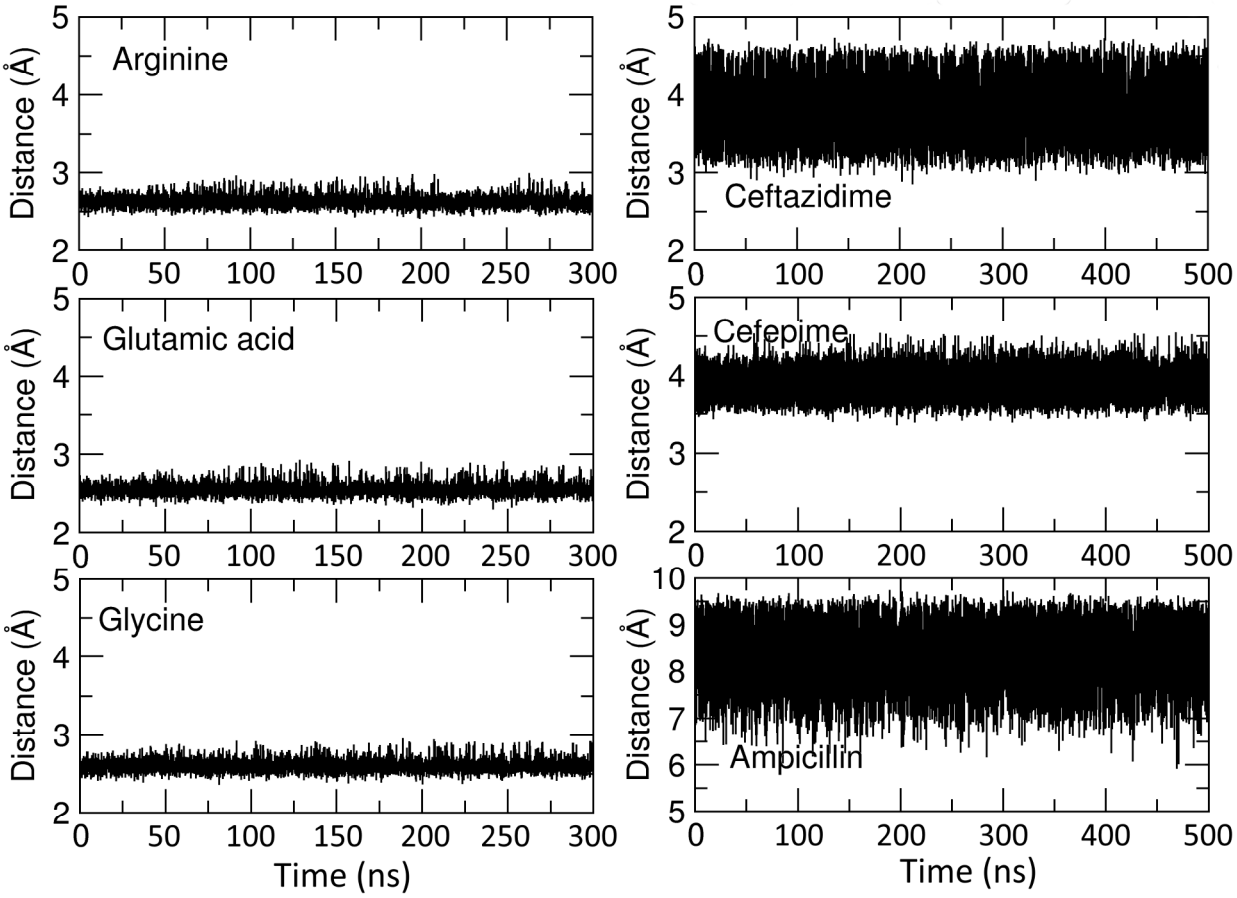

Figure S6. Structures corresponding to the (A) closed and (B) open states of OccK8 as seen from the perplasmic side (left), and from the side (right) of the channel. Loop L3 (orange) and loop L6 (yellow) form the constriction region. Basic residues are shown in blue, acidic residues in red, and the amide residue in green

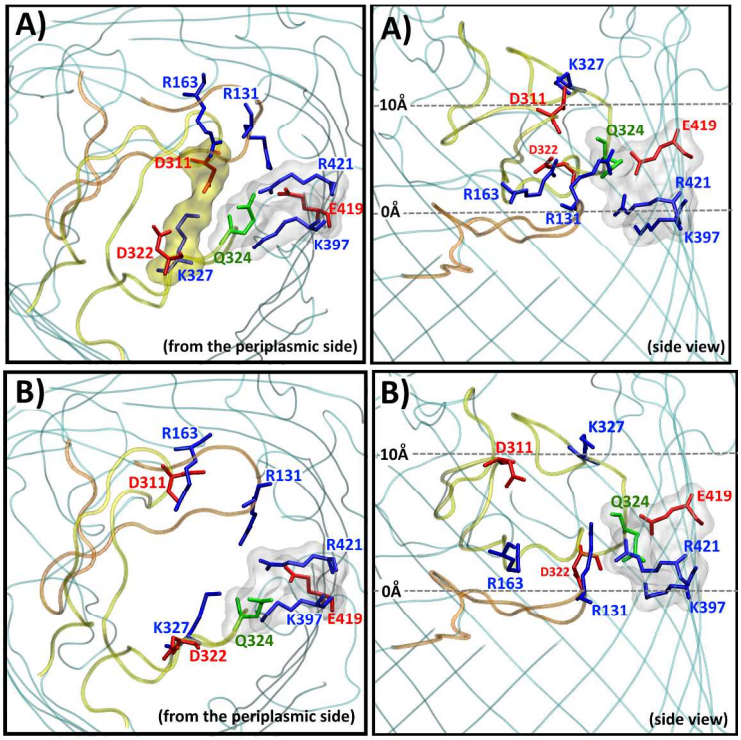

The open and closed states in OccK8. The average area distribution (Figure S2) shows that OccK8 is a fairly small channel with a narrow constriction region and it is supported by its low conductance (Table 1). Clearly, a closed state is dominant for the channel. We have also shown that a favourable substrate can induce structural changes that can significantly increase the available area in the CR resulting in an open state of the channel. We have characterized the structural features responsible for the closed and open states of the pore and they are shown in the figure.

We also discussed the presence of two gates that control the constriction region. Gate A is located at the beginning of the constriction region and it is a result of K327-D311 salt-bridge interaction. This interaction is easily broken in the presence of KCl (Figure S2).

Gate B is in the lower part of the constriction region and it is formed by electrostatic interaction between the members of the basic ladder (R163, R131, R421, K397) with E419 and Q324. The residues R163 and R131 are relatively more flexible than the others which maintain the electrostatic interaction with more stability. The movement of these two residues play a crucial role in gating of the channel. These two residues are on the upper side of the slanted ladder and they tend to interact with the negative charge in a substrate and thus directing them towards the eyelet region. They can move away significantly enlarging the accessible area in the constriction region. Also the movement of R131 towards the extracellular side of the channel is the main reason of the shift in minimal accessible area and its location (Figure 7).

Determination of relative permeabilities of amino acids and antibiotics through OccK8.

Our aim is to investigate to which extend the charged antibiotics/amino acids, which are available in limited quantities, are permeable through the OccK8 channel. To resolve this issue, we apply as previously [1] an experimental electrophysiological tri-ionic zero-current-potential assay. Symmetric low salt concentrations on both sides of the OccK8 containing membrane are supplemented with low concentrations of solutes with the counter ion Na^+ at pH 6 on one site of the membrane (tri-ionic conditions) and the reversal potentials are determined. This setup allows for resolving single channel currents in the range $\ll 10\ pA$. However, since the single channel conductance of the OccK8 channel at low NaCl concentrations is extremely low ($G \cong 1.1\ pS$, at 10 mM NaCl sym., see Figure S8C) we used for our measurement of V_{rev} bilayer containing a very high number of active OccK8 channels. A typical example is shown in Figure S9. Currents (Figure S9A) were recorded by applying the voltage protocol in Figure S9B. From this recording the current amplitude histogram (Figure S9C) is obtained and used to construct the current-voltage relationship (I-V curve) of the bilayer, either as shown in Figure S9 at symmetrical bi-ionic, or asymmetrical tri-ionic conditions (Figure S10).

Using the determined zero-current-potential (V_{rev}) and applying the GHK-current equation (equation (1) below) [1, 2] we then can determine the relative permeability of the involved ion-species (see below).

Experimental conditions for determining relative flux rates for Cefotaxime, Na^+ and Cl^- at pH6:

Cation: $z_{Na^+} = 1;\ c_{K^+cis} = 60\ mM; c_{Na^+\ trans} = 10\ mM$

Anion: $z_{Cl^-} = -1.0;\ c_{Cl^-cis} = 10mM;\ c_{Cl^-trans} = 10mM$

Cefotaxime: $z_{Cefo} = -1;\ c_{Cefo^-cis} = 50mM;\ c_{Cefo^-trans} = 00mM$

Zero current potential: $V_{rev} = 27\ mV\ (experimental\ value)$

Permeability: $P_{Na^+} = 1.55;\ P_{Cl^-} = 1.0$ *(experimental value from bi-ionic recordings of NaCl)*

Considering that the assumptions of the GHK-theory are valid at the given low ion concentrations and the ion fluxes can be regarded as independent of one another we can calculate the current voltage relation for a membrane channel with the above combination of bi-ionic and tri-ionic concentrations using equations 1 to 5 below:

$$(1) \qquad I_x(V, P_X, z, c_{cis}, c_{trans}) = P_x z^2 \frac{VF^2}{RT} \cdot \frac{\left(c_{x,cis} - c_{x,trans} exp\left(\frac{-zFV}{RT}\right)\right)}{1 - exp\left(\frac{-zFV}{RT}\right)}$$

(2) $I_{Na^+}(V) = I(V, P_{K^+}, z_{K^+}, c_{K^+cis}, c_{K^+trans})$,

(3) $I_{CL^-}(V) = I(V, P_{Cl^-}, z_{Cl^-}, c_{Cl^-cis}, c_{Cl^-trans})$

(4) $I_{Cefo^-}(V) = I\left(V, P_{Cefo^-}, z_{Cefo^-}, c_{Cefo^-cis}, c_{Cefo^-trans}\right)$

(5) $\sum I(V) = I_{Na^+}(V) + I_{Cl^-}(V) + I_{Cefo^-}(V)$

The only unknown quantity in equations 1-5, the relative permeability of Cefotaxime (P_{Cefo^-}) is the variable, which can be used to fit the experimental I-V curve to finally obtain the experimental value of V_{rev} (see above). Because of the fit we obtained $P_{Cefo^-} = 0.2$. Thus, the resulting relative permeabilities at the applied tri-ionic conditions were: $P_{Na^+}: P_{Cl^-}: P_{Cefo^-} = 4: 1: 0.2$ (see Table2).

Determination of the Cefotaxime flux-rate through OccK8.

The determined relative permeability's can then be used to calculate the contribution of the individual ions at a given voltage to the total current (equation 1-4, see above). For this we calculate the I-V curves for the normalized total tri-ionic current $\sum I(V) = I_{Na^+}(V) + I_{Cl^-}(V) + I_{Cefo^-}(V)$) and the bi-ionic current $\sum I(V) = I_{Na^+}(V) + I_{Cl^-}(V)$ (Figure 3B).The difference of the two I-V relationships then yields the normalized $I_{Cefo^-}(V)$ current. These normalized currents can be calibrated to the conductance of OccK8 at given experimental conditions (10 mM Cefotaxime cis, 10 mM NaCl sym.) (see Figure S2C). By this procedure, we obtain the I-V relation of OccK8 at the applied conditions (Figure 3C). From the slope of the linear part of this I-V relation we then finally obtain the conductance of OccK8 for Cefotaxime at a 10mM concentration. The flux-rate (n) of Cefotaxime under this condition can then be calculated by: $n = \frac{G_{Cefo} \cdot V_m \cdot N_A}{F}$, ($N_A$ = Avogadro-number and F = Faraday-constant). From this, we finally obtain at V_m= +10 mV a turnover number of n = 110 molecules/s at 10 mM and at 10 µM n= 0.11 molecules/s for the Cefotaxime anion through OccK8.

Single channel conductance of OccK8

The single channel conductance of OccK8 was determined in bilayer containing N≤4 active copies of the OccK8 channel from the current amplitudes of single channel gating events applying a mean variance analysis[3].

Figure S7: (A) Current recording from a bilayer containing three active OccK8 channels ($V_m = +100\,mV$) 500 mM NaCl sym., 20 mM MES pH 6.0 (sym.)**,** (T= 22^0 C). Current recordings were filtered with a 8-pol Bessel filter at 500 Hz. **(B)** Mean variance plot depicting fast channel gating transitions ($f_{gating} = 7.5\,Hz$) of a single OccK8 channel from the open to the closed state in the absence of any effector.

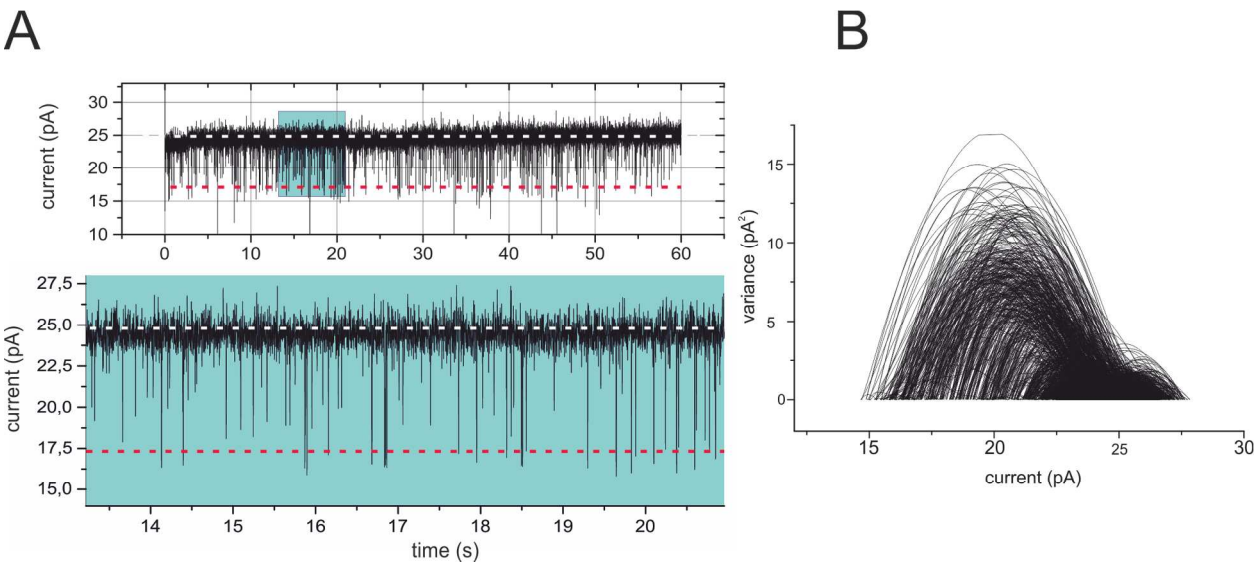

From the corresponding mean variance histogram[3] (data not shown), we obtained current gating transitions with a mean value of $\Delta i = 7.5\,pA$, $V_m = 100\,mV$, corresponding to a mean single channel conductance of $\bar{G}_{single\,channel} = 75\,pS$, at 500 mM NaCl (sym). Moreover, a $i_{max}\ versus\ V_m\ plot$ between $V_m = \pm 100\,mV$ (data not shown) which is a measure of the current through all open channels revealed a total conductance of $\bar{G}_{bilayer} = 224\,pS$, showing that the bilayer contain 3 active OccK8 channels. In the particular case shown in Figure7 two of the channels remained mainly in the fully open state while one channel displayed fast gating. Remarkably, the unusual high intrinsic gating frequency of the OccK8 channel was dependent on the ionic strength of the medium, displaying higher gating frequency at higher NaCl concentrations.

We analysed the OccK8 channel gating amplitudes at the different NaCl concentrations given in table and converted the observed various current amplitude at the given V_m into the corresponding conductance values. In order to avoid counting of non-time-resolved double or triple channel gating transitions we analyzed the data statistically to check the normal distribution of the values (Figure S8).

Figure S8: Statistical analysis of the Occk8 conductance dependence on the NaCl concentration

A. Box chart plot showing the median (line), the mean (open square) and the lower and upper quantile
B. OccK8 single channel conductance at different NaCl concentrations (values from (A))
C. Single channel conductance of OccK8 extrapolated to low NaCl concentrations. Data obtained from the fit in (B)

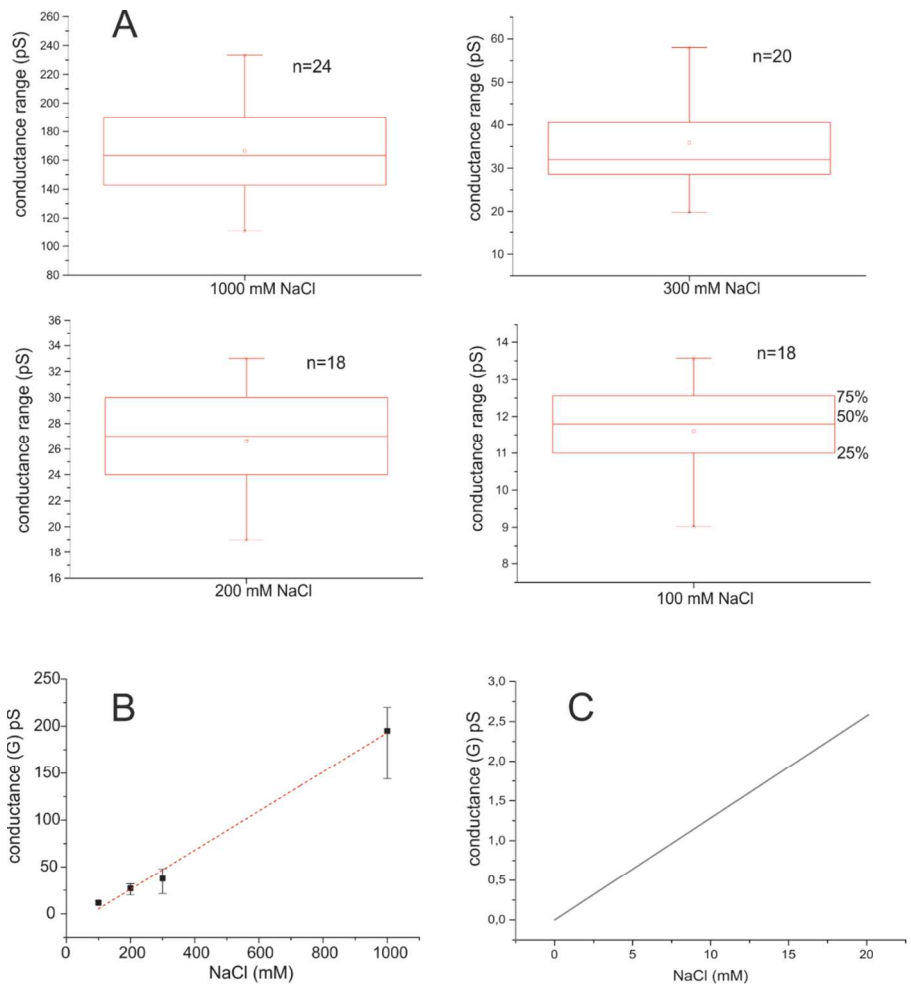

Electrophysiological permeation assay of antibiotics through OprE

To gain further information on permeation of the different substrates through OccK8, we reconstituted monomeric OccK8 into planar lipid bilayer. From single channel recordings where single channel gating events could be resolved (see Figure S7) we determined the single channel conductance of OccK8 (Table S1 in the SI). In 100 mM NaCl the channel revealed a conductance of $\bar{G}_{monomer} = 13\ pS$. This is a rather small conductance value when compared to OmpF ($\bar{G}_{OmpF}^{monomer} = 178\ pS$, at 100 mM NaCl)[4]. Remarkably, this conductance value is even lower than the one observed for most of classical Na^+or K^+channels[2] (e.g. $\bar{G}_{KcsA} = 72\ pS$ at 100 mM KCl)[5]. The conductance ratio of $\frac{G_{OmpF}^{monomer}}{G_{OccK8}^{monomer}} \cong 14$ decreased to about 6 at higher ionic strength (1M NaCl, $\bar{G}_{OmpF}^{monomer} = 940\ pS$)[4], probably due to the opening of Gate A at high salt. Remarkably, the OccK8 channel displayed a rather unusual intrinsic high gating rate from the open to the closed state (Figure S7), which in addition was dependent on the ion concentration, increasing with increasing ion concentration.

For investigating the relative permeability of OccK8 for the anionic substrates ceftazidime, cefotaxime, glutamic acid, carbenicillin and the cationic amino acid arginine we applied an electrophysiological approach based on tri-ionic asymmetric ion concentration on both sites of the OccK8 containing membrane[6-8] Measurements of the current *vs.* voltage (I-V) curves with different substrates under tri-ionic conditions were performed as described in the Materials & Methods section. First, we determined the OccK8 ion selectivity under bi-ionic conditions (Table S1, Figure S7). Remarkably, OccK8 revealed, in contrast to the anion selective other members of the *Pseudomonas aeruginosa* OM carboxylate channels (OccK1-7) subfamily,[9] a slight cation selectivity of $P_{Na^+} / P_{Cl^-} = 1.55$ (Table S1). A representative experimental I-V plot under tri-ionic conditions in the presence of Cefotaxime is shown in Figure S9, while the experimental I-V curves for the other compounds are shown in Figure S11. The reversal potentials (V_{rev}) obtained for the different substrates under tri-ionic conditions are summarized in Table 1.

The experimental V_{rev} values for the different substrates (Table 1) under tri-ionic conditions clearly show that all anionic compounds are permeable through the OccK8 channel, albeit to varying degrees. Selectivity of ion channels is frequently characterized in the framework of the Goldman–Hodgkin–Katz (GHK) voltage equation[2, 10, 11] (equation (1)). The GHK equations were

derived using a one-dimensional Nernst–Planck (1D-NP) equation with the simplifying assumptions that the potential is linear across the length of the pore and that the diffusion coefficients is constant throughout the pore. Those assumptions are certainly not met for OccK8. However, it has been demonstrated for OmpF that the permeability ratios extracted from the GHK equations and the one obtained from BD, MD, and PNP calculations were in excellent accord[12, 13]. Therefore, we consider that it is justified in the first approximation for OccK8 to assume that the ratio of the currents at V_m= 0 mV under asymmetric bi-ionic or tri-ionic conditions can be related to the ratio of the permeability coefficients of the involved ions. We fitted the experimental V_{rev} values using the GHK current equation and obtained the relative permeability value for the different substrates (Table 1). In the next step, we used these values and calculated with the GHK equation the current-voltage curves for a single open OccK8 channel bathed in symmetrical 10 mM NaCl (cis/trans) and 50 mM substrate at the cis compartment. As an example Figure S9B shows the calculated ion current caused by the applied voltage and the concentration gradient of cefotaxime Na. The total current ($i(total) = \sum i_{Na^+} i_{Cl^-} + i_{Cfx^-}$) is carried on one hand by $Na^+$and Cl^- ions $i(NaCl) = \sum i_{Na^+} i_{Cl^-}$ and on the other by cefotaxime anion i_{Cfx^-}. Figure S9C shows the calculated I-V curve for the current carried by the cefotaxime anion (at 10 µM concentration gradient) i_{Cfx^-}. The conductance values for the different substrates calculated in this way are summarized in Table 1.

Figure S9: Current – voltage relationships for OccK8.

- **(A)** Selected experimental I-V curves from bilayers containing multiple copies (control: ~50 OccK8 channels. 10 mM NaCl cis/trans (control (■)) from OccK8 channels and additional 50 mM Na Cefotaxime on cis (electrical ground) side.
- **(B)** Calculated I-V curve using the experimentally measured reversal potential for the given concentration gradient. The black curve is the sum of the ion current originating from the molecule of interest (cefotaxime, blue line) and the ion current carried by Na^+ and Cl^- ions (red line).
- **(C)** Calculated I-V curve for cefotaxime for a single Occk8 channel under tri-ionic conditions. 10 mM NaCl cis/trans and additional 10 µM Na Cefotaxime cis side.

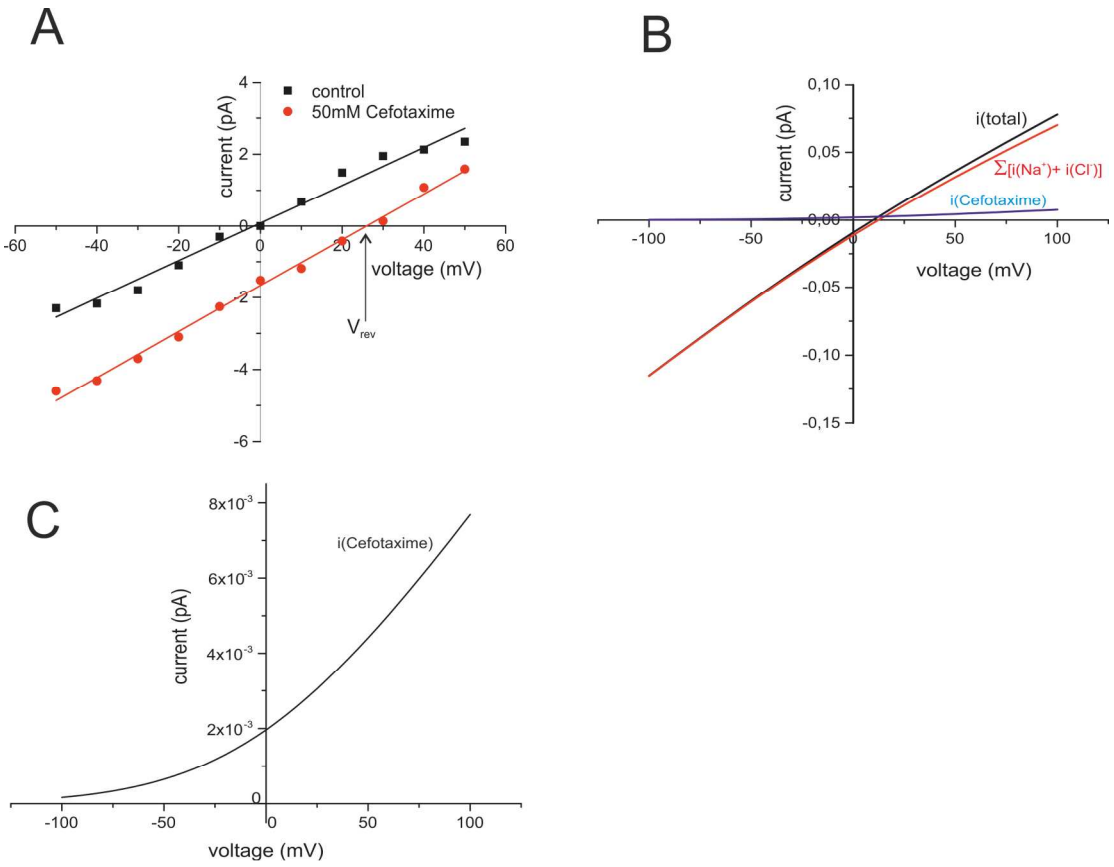
A
control
50mM Cefotaxime
current (pA)
voltage (mV)
V rev
B
i(total)
Σ[i(Na+)+ i(Cl-)]
i(Cefotaxime)
current (pA)
voltage (mV)
C
i(Cefotaxime)
current (pA)
voltage (mV)

Table S1: NaCl conductance of OccK8 at different ionic strength. In the presence of 20 mM MES pH 6.0 (sym.), (T= 22^0 C) (see also Figure S8).

	NaCl (cis/trans)	$\bar{G}_{monomer}$ (pS)	V_{rev} (mV)	P_{Na^+} / P_{Cl^-}
OccK8	1 M / 1M	166.5±24.3 (n=24)	----------	----------
	300 mM / 300mM	35.8 ± 11.9 (n=20)	----------	----------
	200 mM / 200mM	26.6 ± 3.9 (n=18)	----------	----------
	100 mM / 100mM	12.8 ± 3.6 (n=18)	----------	----------
	600mM / 100mM	----------	8 ± 2.5	1.55 :1

Figure S10: Example of the determination of the OccK8 current voltage relationship from multi-channel bilayer at symmetrical 10 mM NaCl, 10 mM Mops pH 6.0 (sym.), (T= 22^0 C). Current recordings were filtered with a 8-pol Bessel filter at 500 Hz.

A. Current recording using the voltage protocol given in (B).
B. Applied voltage protocol for the current recording.
C. Current amplitude histogram for the recording in (A).
D. I-V cure obtained from the mean currents from (C) at the voltages given in (B) line shows the linear fit of the data with a slope conductance of 1.2nS corresponding to ≈1090 active OccK8 channels.

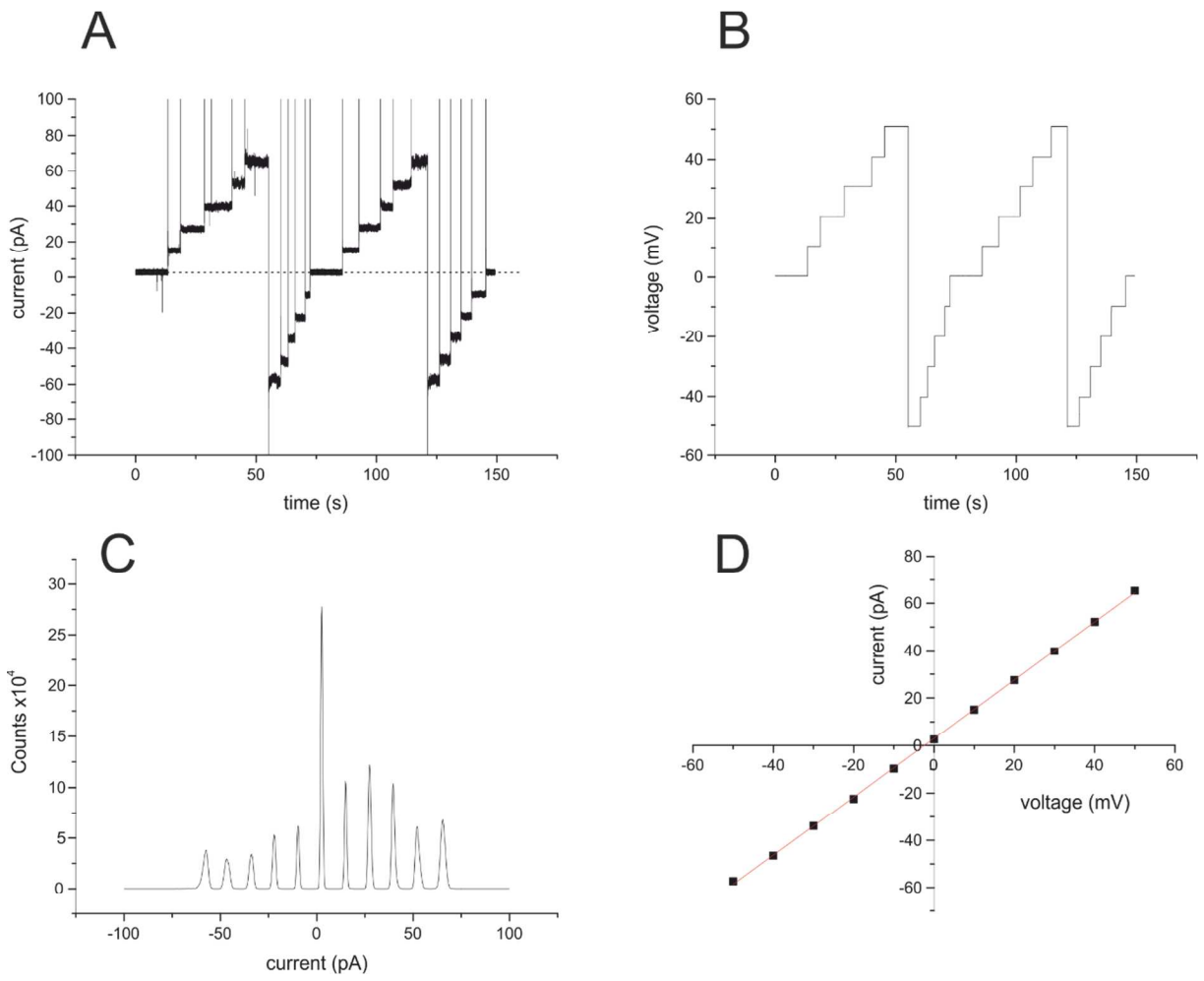

Figure S11: I-V curves for the OccK8 channel under asymmetric tri-ionic conditions, details are given in Table1. Data were obtained from multi-channel bilayer recordings as shown in Figure S9. Lines are linear fits of the data-points. V_{rev} values in Table2 were obtained as indicated in Figure S10A.

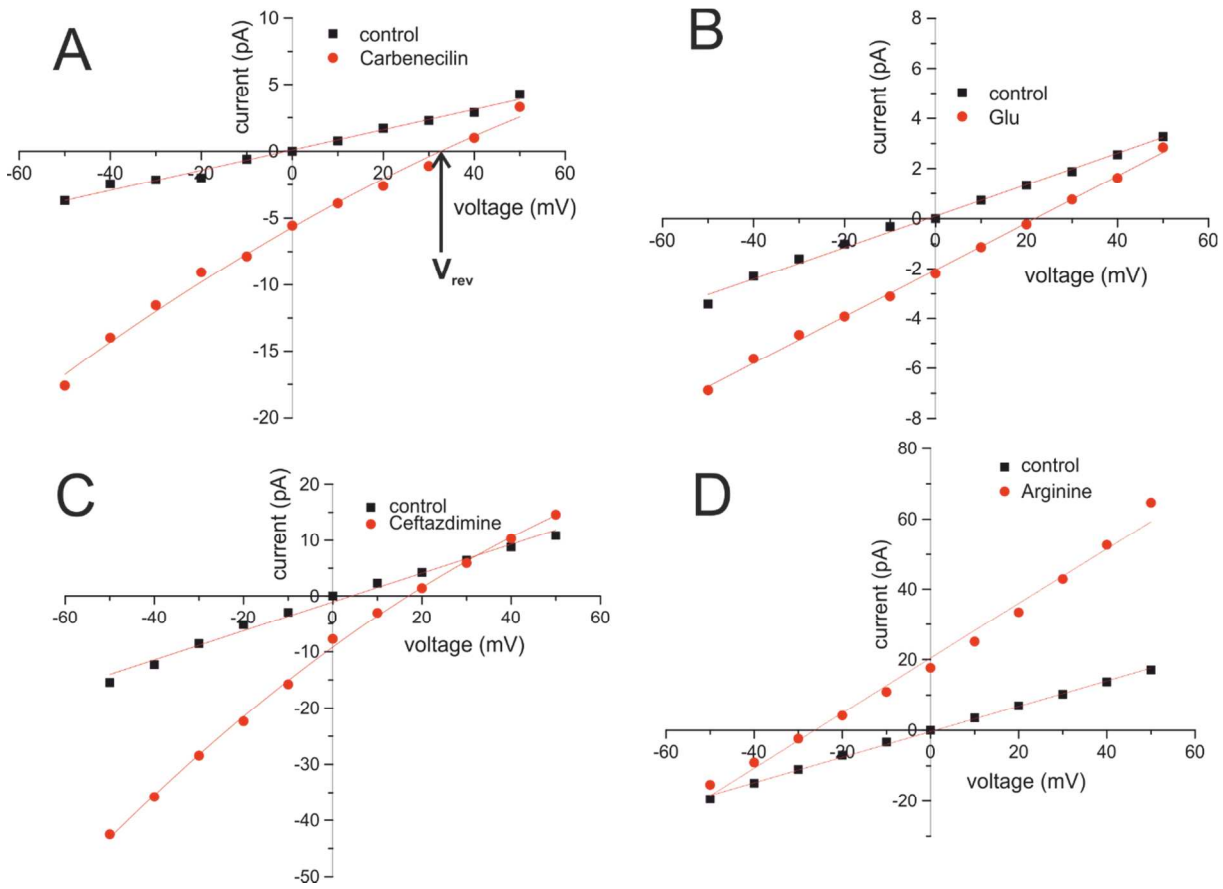

Proteomics procedure

Animal infection models

Intratracheal instillation model: specific pathogen free (SPF) immunocompetent male Sprague-Dawley rats weighing 100 - 120 g or male CD-1 mice weighing 20 - 25 g were infected by depositing an agar bead containing around 10^7 colony-forming units *Pseudomonas aeruginosa* UCBPP-PA14, deep into the lung via nonsurgical intratracheal intubation.[14] In brief, animals were anesthetized with isoflurane (5%) and oxygen (1.5 L/min) utilizing an anesthesia machine. Depth of anesthesia was evaluated by absence of gag reflex; if the reflex was present, the animal was placed back under anesthesia until the reflex disappeared. No animals were utilized until they were fully anesthetized. Animals were infected via intrabronchial instillation of (rats- 100 µl) (mice- 20 µl) molten agar suspension via intratracheal intubation, and then allowed to recover. Animals were returned in their home cages and observed until recovered from anesthesia. At 24 h post infection, animals were sacrificed and lung was homogenized in sterile saline using a lab blender. All procedures are in accordance with protocols approved by the GSK Institutional Animal Care and Use Committee (IACUC), and meet or exceed the standards of the American Association for the Accreditation of Laboratory Animal Care (AAALAC), the United States Department of Health and Human Services and all local and federal animal welfare laws.

Sample workup for proteomics

The sample workup protocol was optimized to deplete host material while maintaining *P. aeruginosa* viability until lysis. All buffers and equipment were used at 0 to 4°C to minimize proteome changes during sample workup. The sample volume (maximum of 1 ml) was estimated and an equal volume of 1% Tergitol in PBS was added followed by vigorous vortexing for 30 s. After centrifugation at 500xg for 5 min, the supernatant was transferred to a fresh tube, and the pellet was extracted again with 2 ml 0.5% Tergitol in PBS. The supernatant was combined with the first supernatant and centrifuged at 18'000xg for 5 min. The pellet was washed with 2 ml and again centrifuged at 18'000xg for 5 min.

The supernatant was removed, and the pellet was resuspended in 100 µL 5% sodium deoxycholate, 5 mM Tris(2-carboxyethyl)phosphine hydrochloride, 100 mM NH_4HCO_3. The

sample was incubated at 90°C for 1 min. and then stored at -80 °C. Samples were thawed and sonicated for 2x20 s (1 s interval, 100% power). Proteins were alkylated with 10 mM iodoacetamide for 30 min in the dark at room temperature. Samples were diluted with 0.1M ammonium bicarbonate solution to a final concentration of 1% sodium deoxycholate before digestion with trypsin (Promega) at 37°C overnight (protein to trypsin ratio: 50:1). After digestion, the samples were supplemented with TFA to a final concentration of 0.5% and HCl to a final concentration of 50 mM. Precipitated sodium deoxycholate was removed by centrifugation at 4°C and 14'000 rpm for 15 min. Peptides in the supernatant were desalted on C18 reversed phase spin columns according to the manufacturer's instructions (Macrospin, Harvard Apparatus), dried under vacuum, and stored at −80°C until further processing.

Parallel reaction monitoring

Heavy proteotypic peptides (JPT Peptide Technologies GmbH) were chemically synthesized for *P. aeruginosa* outer membrane proteins. Peptides were chosen dependent on their highest detection probability and their length ranged between 7 and 20 amino acids. Heavy proteotypic peptides were spiked into each sample as reference peptides at a concentration of 20 fmol of heavy reference peptides per 1 µg of total endogenous protein mass. For spectrum library generation, we generated parallel reaction-monitoring (PRM) assays [15] from a mixture containing 500 fmol of each reference peptide. The setup of the µRPLC-MS system was as described previously [16]. Chromatographic separation of peptides was carried out using an EASY nano-LC 1000 system (Thermo Fisher Scientific) equipped with a heated RP-HPLC column (75 µm x 37 cm) packed in-house with 1.9 µm C18 resin (Reprosil-AQ Pur, Dr. Maisch). Peptides were separated using a linear gradient ranging from 97% solvent A (0.15% formic acid, 2% acetonitrile) and 3% solvent B (98% acetonitrile, 2% water, 0.15% formic acid) to 30% solvent B over 60 minutes at a flow rate of 200 nl/min. Mass spectrometry analysis was performed on Q-Exactive HF mass spectrometer equipped with a nanoelectrospray ion source (both Thermo Fisher Scientific). Each MS1 scan was followed by high-collision-dissociation (HCD) of the 10 most abundant precursor ions with dynamic exclusion for 20 seconds. Total cycle time was approximately 1 s. For MS1, 3e6 ions were accumulated in the Orbitrap cell over a maximum time of 100 ms and scanned at a resolution of 120,000 FWHM (at 200 m/z). MS2 scans were

acquired at a target setting of 1e5 ions, accumulation time of 50 ms and a resolution of 30,000 FWHM (at 200 m/z). Singly charged ions and ions with unassigned charge state were excluded from triggering MS2 events. The normalized collision energy was set to 35%, the mass isolation window was set to 1.1 m/z and one microscan was acquired for each spectrum.

The acquired raw-files were converted to the mascot generic file (mgf) format using the msconvert tool (part of ProteoWizard, version 3.0.4624 (2013-6-3)). Converted files (mgf format) were searched by MASCOT (Matrix Sciences) against normal and reverse sequences (target decoy strategy) of the UniProt database of *P. aeruginosa*, as well as commonly observed contaminants. The precursor ion tolerance was set to 20 ppm and fragment ion tolerance was set to 0.02 Da. Full tryptic specificity was required (cleavage after lysine or arginine residues unless followed by proline), three missed cleavages were allowed, carbamidomethylation of cysteins (+57 Da) was set as fixed modification and arginine (+10 Da), lysine (+8 Da) and oxidation of methionine (+16 Da) were set as variable modifications.

For quantitative PRM experiments the resolution of the orbitrap was set to 30,000 FWHM (at 200 m/z) and the fill time was set to 50 ms to reach a target value of 1e6 ions. Ion isolation window was set to 0.7 Th and the first mass was fixed to 100 Th. Each condition was analyzed in biological triplicates. All raw-files were imported into Spectrodive (Biognosys AG) for protein and peptide quantification. We normalized protein abundance based on OprF (at 775 fmol / µg *P. aeruginosa* tryptic peptides), which is constitutively present under widely varying conditions. Quantification based on CFU counts was less accurate, presumably because of aggregates that would still give raise to single colonies.

References

1. Ghai, I.; Pira, A.; Scorciapino, M. A.; Bodrenko, I.; Benier, L.; Ceccarelli, M.; Winterhalter, M.; Wagner, R., General Method to Determine the Flux of Charged Molecules through Nanopores Applied to beta-Lactamase Inhibitors and OmpF. *J Phys Chem Lett* **2017**, 1295-1301. DOI: 10.1021/acs.jpclett.7b00062.
2. Hille, B., *Ionic Channels of Excitable Membranes*. Sinauer Ass. Inc.: Sunderland, Ma 01375, 2001; Vol. 3.
3. Patlak, J. B., Measuring kinetics of complex single ion channel data using mean-variance histograms. *Biophysical journal* **1993,** *65* (1), 29-42. DOI: 10.1016/S0006-3495(93)81041-5.
4. Danelon, C.; Suenaga, A.; Winterhalter, M.; Yamato, I., Molecular origin of the cation selectivity in OmpF porin: single channel conductances vs. free energy calculation. *Biophys Chem* **2003,** *104* (3), 591-603.

5. Meuser, D.; Splitt, H.; Wagner, R.; Schrempf, H., Exploring the open pore of the potassium channel from Streptomyces lividans. *FEBS Letters* **1999,** *462* (3), 447-52.
6. Citak, F.; Ghai, I.; Rosenkötter, F.; Benier, L.; Winterhalter, M.; Wagner, R., Probing transport of fosfomycin through substrate specific OprO and OprP from Pseudomonas aeruginosa. *Biochemical and biophysical research communications* **2017**.
7. Ghai, I.; Pira, A.; Scorciapino, M.; Bodrenko, I.; Benier, L.; Ceccarelli, M.; Winterhalter, M.; Wagner, R., A General Method to Determine the Flux of Charged Molecules Through Nanopores Applied to ß-Lactamase Inhibitors and OmpF. *The journal of physical chemistry letters* **2017**.
8. Ghai, I.; Winterhalter, M.; Wagner, R., Probing transport of charged β-lactamase inhibitors through OmpC, a membrane channel from E. coli. *Biochemical and Biophysical Research Communications* **2017,** *484* (1), 51-55.
9. Liu, J.; Eren, E.; Vijayaraghavan, J.; Cheneke, B.; Indic, M.; van den Berg, B.; Movileanu, L., OccK Channels from Pseudomonas aeruginosa Exhibit Diverse Single-Channel Electrical Signatures but Conserved Anion Selectivity. *Biochemistry* **2012,** *51* (11), 2319-2330. DOI: 10.1021/bi300066w.
10. Hodgkin, A. L.; Katz, B., The effect of sodium ions on the electrical activity of the giant axon of the squid. *J Physiol* **1949,** *108* (1), 37-77.
11. Goldman, D. E., Potential, Impedance, and Rectification in Membranes. *Journal of General Physiology* **1943,** *21* (1), 37-60. DOI: 10.1085/jgp.27.1.37.
12. Im, W.; Roux, B., Ion permeation and selectivity of OmpF porin: a theoretical study based on molecular dynamics, Brownian dynamics, and continuum electrodiffusion theory. *Journal of molecular biology* **2002,** *322* (4), 851-869.
13. Khalili-Araghi, F.; Ziervogel, B.; Gumbart, J. C.; Roux, B., Molecular dynamics simulations of membrane proteins under asymmetric ionic concentrations. *The Journal of general physiology* **2013,** *142* (4), 465-475.
14. Hoover, J. L.; Lewandowski, T. F.; Mininger, C. L.; Singley, C. M.; Sucoloski, S.; Rittenhouse, S., A Robust Pneumonia Model in Immunocompetent Rodents to Evaluate Antibacterial Efficacy against S. pneumoniae, H. influenzae, K. pneumoniae, P. aeruginosa or A. baumannii. *J Vis Exp* **2017,** (119). DOI: 10.3791/55068.
15. Peterson, A. C.; Russell, J. D.; Bailey, D. J.; Westphall, M. S.; Coon, J. J., Parallel reaction monitoring for high resolution and high mass accuracy quantitative, targeted proteomics. *Mol Cell Proteomics* **2012,** *11* (11), 1475-88. DOI: 10.1074/mcp.O112.020131.
16. Ahrne, E.; Glatter, T.; Vigano, C.; Schubert, C.; Nigg, E. A.; Schmidt, A., Evaluation and Improvement of Quantification Accuracy in Isobaric Mass Tag-Based Protein Quantification Experiments. *J Proteome Res* **2016,** *15* (8), 2537-47. DOI: 10.1021/acs.jproteome.6b00066.